

## Experimental synchronization of spatiotemporal chaos in nonlinear optics

P. L. Ramazza, U. Bortolozzo,\* and S. Boccaletti

*Istituto Sistemi Complessi CNR, Largo E. Fermi, 6 150125 Florence, Italy*

(Received 10 February 2005; revised manuscript received 14 September 2005; published 21 March 2006)

We demonstrate that a unidirectional coupling between a pattern forming system and its replica induces complete synchronization of the slave to the master system onto a spatiotemporal chaotic state.

DOI: [10.1103/PhysRevE.73.036213](https://doi.org/10.1103/PhysRevE.73.036213)

PACS number(s): 05.45.Xt, 42.40.Eq, 42.65.Sf

In recent years, synchronization of complex systems has attracted great interest in the scientific community [1] as well as lay audiences [2]. This indicates the behavior of two (or many) systems (either equivalent or nonequivalent) that adjust a common feature of their complex dynamics due to coupling or forcing.

For time chaotic systems, four types of synchronization have mostly been studied, namely, complete (CS), phase (PS), lag (LS), and generalized synchronization (GS). CS refers to a process whereby two interacting systems perfectly link their chaotic trajectories, thus remaining in step with each other in the course of the time [3]. GS implies the hooking of the output of one system to a given function of the output of the other system [4]. PS is characterized by a locking of the phases of the two signals, also in the absence of a substantial correlation between the two chaotic amplitudes [5]. Finally, LS consists in the hooking of one system to the lagged output of the other [6]. All these effects have been explored in natural phenomena [7], and laboratory experiments [8], and unified approaches to describe [9] and measure synchronization states have been proposed.

When the interest shifted to space-extended systems, synchronization phenomena were shown in large populations of coupled chaotic units and neural networks [10], globally or locally coupled map lattices [11], and pattern forming systems governed by partial differential equations [12]. Here, however, all theoretical and numerical progresses were accompanied by a substantial lack of experimental verifications. Precisely, CS of spatiotemporal patterns was first observed in chemistry [13] for two mutually coupled Belousov-Zhabotinski cells, where, however, the resulting synchronized state corresponded to the suppression of spatiotemporal complexity and the emergence of a common spiral behavior. Later on, LS was observed in a pair of unidirectionally coupled nonlinear optical systems [14]. The evidence here was given in terms of an improvement in the lagged correlation between the master and slave patterns. Finally, GS was demonstrated in an open loop liquid crystal light modulator with optoelectronic feedback [15] by the use of the so-called auxiliary system method [4].

In this paper we report direct experimental evidence of complete synchronization on unidirectionally coupled pattern forming systems. At variance with what observed in Ref. [13], the resulting synchronized state here corresponds to a

spatiotemporal chaotic dynamics where the slave system is identically attained to the behavior of the master system.

Our research makes use of the same experimental system of Ref. [16]: a liquid crystal light valve (LCLV) with optical feedback, and an extra optoelectronic control feedback loop. In Ref. [16], we demonstrated the ability of the control loop in targeting desired unstable stationary states of the dynamics. The time needed to target a given state was of the order of a few (2–3) s (see Fig. 3 of Ref. [16]). Our purpose here is instead to control a continuously time evolving dynamics, that is a time sequence of snapshots separated in time by few hundreds of ms (typically 200–300 ms). In light of our previous results, this would not be possible if the successive snapshots were mutually uncorrelated. However, as we will show in the following, the task can be accomplished for a target dynamics that reproduces a portion of the natural (uncontrolled) evolution of the system, where each snapshot maintains a certain degree of correlation with the previous one.

The experimental setup is sketched in Fig. 1. A main optical feedback loop (MOFL) consists of a liquid crystal light valve (LCLV) with optical feedback [17]. The LCLV induces on the reading light a phase delay depending on the writing intensity. This dependence is of simple proportionality (Kerr-like effect) for all experimental parameters used in the present investigation (see Fig. 1, lower part). The pattern forming mechanism acts on an homogeneous pump wave of intensity  $I_p$  sent onto the front face of the LCLV. The wave is totally reflected and acquires a spatial phase modulation. Diffractive propagation along the MOFL provides conversion of phase into amplitude modulations. Due to the Kerr-like behavior of the LCLV, these amplitude modulations are converted back to phase modulations, so that eventually a positive feedback establishes for some spatial frequencies, which are destabilized resulting in pattern formation.

An additional electro-optic control loop is constituted by a video-camera and a personal computer driving a liquid crystal display (LCD). The control signal is a laser beam that traverses the LCD before being injected into the MOFL. The LCD display is operating in transmission, and encodes linearly the gray level images output by the PC, onto the laser beam traversing it.

When the control loop is open, the dynamics of the optical beam phase  $\phi(x, y, t)$  at the LCLV output can be described by [18,19]  $\frac{\partial \phi}{\partial t} = -\frac{1}{\tau}(\phi - \phi_0) + D\nabla^2 \phi + \alpha I_{fb}$ , where  $\phi_0$  is the working reference phase,  $\tau$  the LCLV relaxation time,  $D$  a diffusion coefficient,  $\alpha$  the LCLV nonlinearity strength,

\*Also at Institut Non Lineaire de Nice, France.

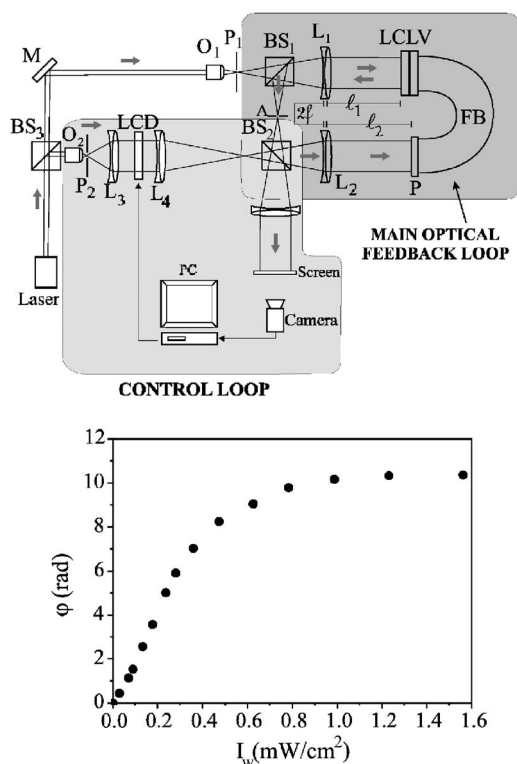


FIG. 1. Upper part: Experimental setup. The main optical feedback loop is generating the unperturbed space-time chaotic dynamics. An extended laser beam is sent in a closed loop containing a nonlinear Kerr-like medium operating in reflection (liquid crystal light valve). Instabilities develop in the transverse plane of the beam. *M*: mirror; *O*<sub>1</sub>: microscope objectives; *P*<sub>1</sub>: pinhole; *A*: aperture; *BS*<sub>1</sub>, *BS*<sub>2</sub>: beam splitters; *LCLV*: liquid crystal light valve; *L*<sub>1</sub>, *L*<sub>2</sub>: lenses of focal lens *f*; *L*<sub>3</sub>: additional lens; *FB*: fiber bundle. In our experiment, the effective free propagation length from the front face of the LCLV to the plane *P* is  $2f - (l_1 + l_2) = +90$  mm. The light distribution at *P* is transported by the fiber bundle to the rear plane of the LCLV. Control loop: *O*<sub>2</sub>: microscope objectives; *P*<sub>2</sub>: pinhole; *BS*<sub>3</sub>: beam splitters; *LCD*: liquid crystal display; *L*<sub>3</sub>, *L*<sub>4</sub>: lenses; *P*: input plane of the fiber bundle. The lenses *L*<sub>4</sub> and *L*<sub>2</sub> form a 1:1 image of the LCD onto the plane *P*. The arrows indicate the local direction of light propagation. Lower part: Open loop characteristic of the LCLV. The plot reports  $\phi$  (the phase induced on the reading beam, in radians) vs  $I_w$  (the writing intensity sent to the valve, in  $\text{mW}/\text{cm}^2$ ). In all our measurements,  $I_w$  (named  $I_{fb}$  in the closed loop configuration) is kept smaller than  $0.4 \text{ mW}/\text{cm}^2$ . Therefore, the valve is always operating in the proportionality (so called Kerr) regime.

and  $I_{fb}(x, y, t)$  the feedback intensity at the input plane of the FB.  $I_{fb}$  is a nonlinear (and nonlocal) function of the phase  $\phi$  [18,19].

With increasing the pump intensity  $I_p$  above the threshold  $I_{thr}$  of pattern formation, which is of  $90 \mu\text{W}/\text{cm}^2$  for the parameters used, the homogeneous solution destabilizes, and an hexagonal pattern arises. This allows to introduce a reduced pump parameter  $I \equiv \frac{I_p}{I_{thr}}$ . A further increase in  $I$  above unity leads eventually to a destabilization of hexagons in favor of a regime of space-time chaos (STC) [18,20]. An aperture *A* (located in a Fourier plane of the MOFL) has the

role of limiting the spatial frequency bandwidth *B* of the system, which is another control parameter. Throughout the experiment reported here, *B* is kept fixed at 1.5 times the diffractive spatial frequency of the system. This is the frequency of the hexagonal pattern which bifurcates at the threshold for pattern formation.

When the control loop is closed, a fraction of  $I_{fb}$  is extracted and detected by a video camera, which is interfaced to a personal computer (PC) via a frame grabber. The PC processes the input image, and sends a driving signal to the LCD, upon which a plane beam of intensity  $I_0$  incides. The transfer function  $T(x, y, t)$  of the LCD is the sum of a constant mean transfer coefficient  $T_0$  and a modulation signal  $s(x, y, t)$ , which we set to be proportional to the error signal between the actual pattern intensity  $I_{fb}$ , and a desired time dependent target pattern  $I_T(x, y, t)$   $\{s(x, y, t) = -(\gamma/I_0) \times [I_{fb}(x, y, t) - I_T(x, y, t)]\}$ . Further real time processing performed by the PC includes the evaluation of *s*, and the calculation of the cross-correlation between  $I_{fb}$  and  $I_T$ . The resulting actualization time for *s* is of the order of 200 to 300 ms, to be compared with the characteristic time of the pattern dynamics (of the order of 1 s for the parameters used in our experiment). The diffractive scale of the system is  $\sqrt{2\lambda L} \approx 300 \mu\text{m}$  ( $\lambda = 514 \text{ nm}$  being the laser wavelength, and  $L = 90 \text{ mm}$  the free propagation length in the MOFL). On the other side, the control area is  $\approx 2000 \times 2000 \mu\text{m}^2$ , and the control signal is made of  $128 \times 128$  pixels. This grants us a spatial resolution of  $\approx 20$  pixels per typical pattern wavelength.

With the help of such real-space real-time control technique we have recently given evidence that two-dimensional stationary target patterns with arbitrary symmetries and shapes can be effectively and robustly stabilized within STC [16]. Here, instead, we aim to demonstrating complete synchronization in a unidirectionally coupled scheme between two identical systems in a regime of STC. For this purpose, we initially let the control loop open and record (over a time interval *T*) the free evolution of the system for a value of *I* at which the uncontrolled dynamics displays STC. A qualitative characterization of the resulting dynamics has been given in Ref. [16]. The signal consists basically of a set of closely packed diffractive spots, evolving in space and time in an unpredictable way.

After the registration of this dynamics, which we refer to as the master dynamics (MD) henceforth, further free evolution is granted to the uncontrolled system, so that after a few seconds the configuration of the MOFL output is totally uncorrelated with the initial frame of the MD. At this point, we close the control loop and replay the registered MD as the target pattern  $I_T(x, y, t)$ . In this way, we are implementing a unidirectional coupling scheme between two identical systems starting from fully uncorrelated initial conditions. By repeating the replaying procedure of the MD with increasing values of  $\gamma$  (hereinafter called the coupling strength parameter), we eventually observe full synchronization between the controlled output of the MOFL [the slave dynamics (SD)] and the MD.

Complete synchronization between SD and MD is shown in Fig. 2, reporting the space (vertical)-time (horizontal) dy-

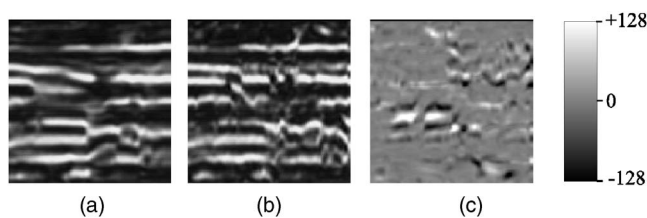


FIG. 2. Space (vertical)-time (horizontal) dynamical evolution at  $I=3$  of a line of (a) the output free running signal from the MOFL (master dynamics); (b) the slave dynamics in conditions of closed control loop; (c) the synchronization error, corresponding to the difference of (a) and (b). The gray scale in (c) is the one shown in the band at right, such that black corresponds to negative values, white to positive values and gray to values close to 0.

namical evolution of the central vertical line of pixels for the master dynamics 2(a), slave dynamics 2(b) and the difference between the two, 2(c). Figure 2 is taken at  $\gamma=0.8$ , and shows how the SD closely follows the MD at any time during control. As visible in Fig. 2(c), the synchronization error  $E(x, y, t) = I_{fb}(x, y, t) - I_T(x, y, t)$  is close to vanishing nearly always and everywhere in time as a result of the complete synchronization process.

Notice that the final CS state is here realized within a full STC regime, at variance with what reported in Ref. [13] for a bidirectional coupling between two excitable media, where the emergence of synchronization was associated with the suppression of space-time chaos in the system.

A quantitative measurement of CS can be given by monitoring the behavior of the time dependent cross-correlation function  $C(t) = \langle I_{fb}(\mathbf{r}, t) \cdot I_T(\mathbf{r}, t) \rangle_{\mathbf{r}}$  between the instantaneous patterns in the SD and MD during the synchronization process [ $\langle \dots \rangle_{\mathbf{r}}$  denotes here a spatial average in the plane  $\mathbf{r} \equiv (x, y)$ ].  $C(t)$  is by definition vanishing for linearly uncorrelated systems, whereas  $C(t) \sim 1$  for fully synchronized dynamics.

Figure 3 reports the temporal behavior of  $C(t)$  for  $I=3$  and for three different values of the coupling strength [(a)  $\gamma=0.24$ , (b)  $\gamma=0.4$ , and (c)  $\gamma=0.8$ ]. In all horizontal axes,  $t=0$  has been taken as the instant at which the MD starts to be replayed in the control loop. A first important observation is that the cross correlation starts from a nonvanishing value at  $t=0$ . This is because the uncontrolled STC dynamics has a non zero mean field, as it can be appreciated from inspection of Figs. 2(a) and 2(b). Namely, the uncoupled MD and SD have a certain degree of “phase rigidity,” i.e., even if there are chaotic fluctuations, bright (dark) areas remain more or less bright (dark) for most of time. Similar properties have been observed experimentally and discussed in various other cases of space extended systems giving rise to STC dynamics [21].

At low values of the coupling strength ( $\gamma=0.24$ ), no synchronization is set in the system. This is visible in Fig. 3(a), where  $C(t)$  experiences large fluctuations in time around a mean value not substantially different from the initial correlation level. For intermediate coupling strengths [ $\gamma=0.4$  in Fig. 3(b)], a partial synchronization emerges in the system after a transient time, though several deviations of the SD from the MD still remain, reflected by the rather large fluctuations

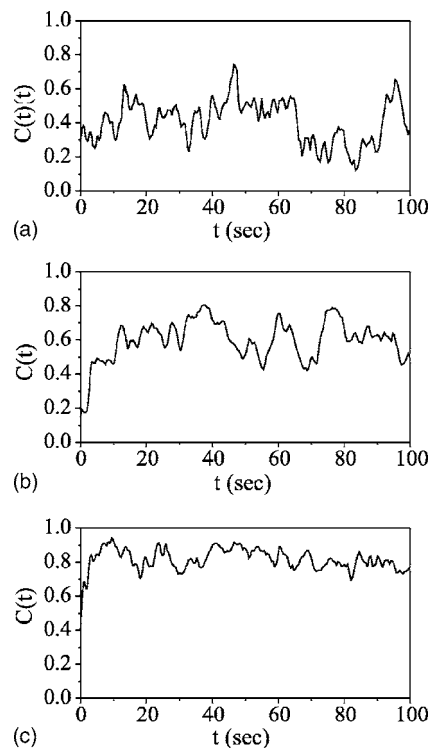


FIG. 3. Cross correlation function  $C(t)$  (see text for definition) vs time during some synchronization trials for  $I=3$ . (a)  $\gamma=0.24$ , (b)  $\gamma=0.40$ , (c)  $\gamma=0.8$ . In all cases  $t=0$  indicates the instant at which the MD starts to be replayed in the control loop.

tuations around the asymptotic value of  $C(t)$  visible in Fig. 3(b). Finally, a further increase in  $\gamma$  induce a full CS in the system [see the case  $\gamma=0.8$  in Fig. 3(c)], where the asymptotic value of the cross correlation approaches unity, and the residual fluctuations in  $C(t)$  shrink considerably. Notice that, as  $\gamma$  increases, the transient time before reaching CS decreases. The global picture depicted in Fig. 3 confirms that CS here is a threshold phenomenon, as it was introduced originally for time-chaotic systems [3].

The global scenario of observed CS is illustrated in Fig. 4, where the time average of the cross correlation function  $C = \langle C(t) \rangle_T$  ( $\langle \dots \rangle_T$  here denotes a further time average over the full time interval  $T$ ) is reported vs the coupling strength at different values of pump intensities  $I$ . In all cases, our

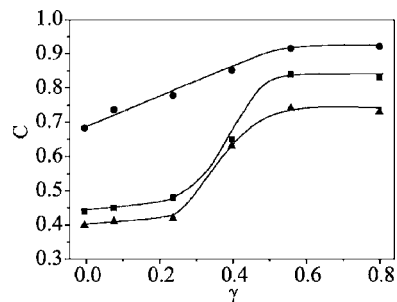


FIG. 4. Time average cross correlation function  $C$  (see text for definition) vs the coupling strength  $\gamma$  for  $I=2$  (circles),  $I=3$  (squares), and  $I=4$  (triangles). In all cases, the solid lines connecting points are drawn as guides for the eyes.

proposed coupling scheme is effective in inducing CS, as  $C$  considerably increases with  $\gamma$  with respect to the corresponding uncoupled values. An increase in the pump intensity  $I$  leads to a progressive deterioration of CS, reflected by smaller asymptotic values of  $C(t)$ .

For low values of  $I$  ( $I \approx 2$ ), the system is not yet in the regime of fully developed space-time chaos; hence the curve for  $I=2$  in Fig. 4 starts at a rather high value of correlation already at  $\gamma=0$ , and regularly increases to  $C \approx 0.9$  for  $\gamma = 0.8$ , without marking a clear transition point to synchronization. At variance, the system is in a regime of developed space-time chaos for higher values of  $\gamma$  ( $\gamma \gtrsim 3$ ). In this latter condition, one can observe that the curves of Fig. 4 start at low values of correlation, and increase for increasing  $\gamma$  with a change of slope around  $\gamma=0.4$ , where the transition to synchronization occurs. As a consequence, the transition from the qualitative behavior of  $C(\gamma)$  for  $I=2$  to that for  $I=3, 4$  is of smooth type.

A measurable increasing of  $C$  with  $\gamma$  is observed for all values of  $I \leq 5$ . For  $I > 5$  the failing of synchronization is due to the fact that the self-correlation time of the natural dynamics becomes comparable with (or even smaller than) the control loop time resolution, eventually deteriorating the control efficiency in the experiment.

Another factor limiting the control efficiency is the spatial resolution of the control signal, to be compared with the

smaller spatial scales emerging in the uncontrolled dynamics. In our experiment, the space-time chaotic states can be synchronized (i.e.,  $C \gtrsim 0.5$  for  $\gamma \approx 0.6-0.8$ ) for all values of  $B \leq 2.2$ , while for higher  $B$  the high spatial frequencies in the signal are not efficiently managed by the control loop.

Numerical simulations of the model equations give full qualitative confirmation of the experimental scenario. From a quantitative point of view, the values of  $C$  obtained in the numerics are typically 10–20 % higher than the corresponding experimental ones, reflecting the presence in the experimental system of some spatial inhomogeneities, which limits the values of the correlation obtainable.

In conclusion, we have demonstrated that a unidirectional coupling between two identical pattern forming systems induces complete synchronization of the slave to the master dynamics, with a resulting synchronized behavior corresponding to a spatiotemporal chaotic state. Though realized with a nonlinear optical experiment, the coupling scheme used (based on a real-space real-time control of a recorded and replayed space-time chaotic dynamics) can in principle be implemented in many other physical and chemical pattern forming systems.

This work was partly supported by MIUR-FIRB Project No. RBNE01CW3M-001.

- 
- [1] S. Boccaletti, J. Kurths, G. Osipov, D. Valladares, and C. Zhou, *Phys. Rep.* **366**, 1 (2002).
- [2] S. Strogatz, *Sync: The Emerging Science of Spontaneous Order* (Hyperion Press, New York, 2003).
- [3] H. Fujisaka and T. Yamada, *Prog. Theor. Phys.* **69**, 32 (1983); L. M. Pecora and T. L. Carroll, *Phys. Rev. Lett.* **64**, 821 (1990).
- [4] L. Kocarev and U. Parlitz, *Phys. Rev. Lett.* **76**, 1816 (1996).
- [5] M. G. Rosenblum, A. S. Pikovsky, and J. Kurths, *Phys. Rev. Lett.* **76**, 1804 (1996).
- [6] M. G. Rosenblum, A. S. Pikovsky, and J. Kurths, *Phys. Rev. Lett.* **78**, 4193 (1997); S. Boccaletti and D. L. Valladares, *Phys. Rev. E* **62**, 7497 (2000).
- [7] C. Schafer, M. G. Rosenblum, J. Kurths, and H. H. Abel, *Nature (London)* **392**, 239 (1998); G. M. Hall, S. Bahar, and D. J. Gauthier, *Phys. Rev. Lett.* **82**, 2995 (1999).
- [8] K. M. Cuomo and A. V. Oppenheim, *Phys. Rev. Lett.* **71**, 65 (1993); R. Roy and K. S. Thornburg, *ibid.* **72**, 2009 (1994); D. Maza, A. Vallone, H. Mancini, and S. Boccaletti, *ibid.* **85**, 5567 (2000).
- [9] R. Brown and L. Kocarev, *Chaos* **10**, 344 (2000); S. Boccaletti, Louis M. Pecora, and A. Pelaez, *Phys. Rev. E* **63**, 066219 (2001).
- [10] S. H. Strogatz, R. E. Mirollo, and P. C. Matthews, *Phys. Rev. Lett.* **68**, 2730 (1992); D. H. Zanette, *Phys. Rev. E* **55**, 5315 (1997); V. N. Belykh, I. V. Belykh, and M. Hasler, *ibid.* **62**, 6332 (2000).
- [11] V. N. Belykh and E. Mosekilde, *Phys. Rev. E* **54**, 3196 (1996); A. Pikovsky, O. Popovych, and Yu. Maistrenko, *ibid.* **87**, 044102 (2001).
- [12] L. Kocarev, Z. Tasev, and U. Parlitz, *Phys. Rev. Lett.* **79**, 51 (1997); S. Boccaletti, J. Bragard, F. T. Arecchi, and H. Mancini, *ibid.* **83**, 536 (1999).
- [13] M. Hildebrand, J. Cui, E. Mihaliuk, J. Wang, and K. Showalter, *Phys. Rev. E* **68**, 026205 (2003).
- [14] R. Neubecker and B. Gütlich, *Phys. Rev. Lett.* **92**, 154101 (2004).
- [15] E. A. Rogers, R. Kalra, R. D. Schroll, A. Uchida, D. P. Lathrop, and R. Roy, *Phys. Rev. Lett.* **93**, 084101 (2004).
- [16] L. Pastur, L. Gostiaux, U. Bortolozzo, S. Boccaletti, and P. L. Ramazza, *Phys. Rev. Lett.* **93**, 063902 (2004).
- [17] S. A. Akhmanov, M. A. Vorontsov, and V. Yu Ivanov, *JETP Lett.* **47**, 707 (1988).
- [18] G. D'Alessandro and W. J. Firth, *Phys. Rev. Lett.* **66**, 2597 (1991).
- [19] R. Neubecker, G. L. Oppo, B. Thuring, and T. Tschudi, *Phys. Rev. A* **52**, 791 (1995).
- [20] R. Neubecker, B. Thuring, M. Kreuzer, and T. Tschudi, *Chaos, Solitons Fractals* **10**, 681 (1999).
- [21] B. J. Gluckman, P. Marcq, J. Bridger, and J. P. Gollub, *Phys. Rev. Lett.* **71**, 2034 (1993); Li Ning, Y. Hu, R. E. Ecke, and G. Ahlers, *ibid.* **71**, 2216 (1993); S. Rudroff and I. Rehberg, *Phys. Rev. E* **55**, 2742 (1997).